Thermal conductivity tensor of NbO_2

Hai Jun Cho[1,2]*, Gowoon Kim[2,3+], Takaki Onozato[2+], Hyoungjeen Jeen[3], and Hiromichi Ohta[1,2]

[1]*Research Institute for Electronic Science, Hokkaido University, N20W10, Kita, Sapporo 001−0020, Japan*

[2]*Graduate School of Information Science and Technology, Hokkaido University, N14W9, Kita, Sapporo 060−0814, Japan*

[3]*Department of Physics, Pusan National University, Busan 46241, South Korea*

[+]Equally contributed to this work

*To whom all correspondence should be addressed: H.J.C (joon@es.hokudai.ac.jp)

Abstract

Among several transition metal oxides showing metal to insulator transition, NbO_2 has attracted attention as the active material of memory devices due to its high thermal stability. Although clarification of thermal conductivity (κ) is essentially important for optimizing the NbO_2 device performance, it has not been reported thus far probably due to the anisotropic crystal structure. Here we show the thermal conductivity tensor of NbO_2 crystal. We measured the thermal conductivities of (110)-, (001)-, and (111)-oriented NbO_2 films and found <111>-direction shows ~1 W m^{-1} K^{-1} higher thermal conductivity compared with the other directions (~3 W m^{-1} K^{-1}). Using the measured κ-values, we successfully determined thermal conductivity tensor components κ_{11}, κ_{13}, and κ_{33}. The diagonal components of the thermal conductivity tensor were ~2.5 W m^{-1} K^{-1}

while the nonzero off-diagonal component was ~1 W m^{-1} K^{-1}. We believe that the present results are of great value in optimizing the performance of NbO_2 based devices.

Introduction

Transition metal oxides exhibiting metal-to-insulator transitions (MIT) are considered to be promising candidates for next generation non-volatile resistive random-access memory (RRAM) applications [1-4]. As memory devices are constantly exposed to read/reset pulses, they are always exposed to high heat accumulation rates, and thermal stability is one of the key issues in the materials selection [5]. For this reason, NbO_2 is gaining interest in the RRAM community [6-10] since it has high MIT temperature (~1080 K) [11-12] and therefore high thermal stability. The approaches vary from local joule heating [13-14] to utilizing electroforming current to change its oxidation states [15-16]. In all cases, understanding the thermal conductivity of NbO_2 is essential for the device optimization. However, it has been largely overlooked compared to the electrical properties because there is a lack of studies in literature on the thermal conductivity characterization of NbO_2.

One of the difficulties in measuring the thermal conductivity of NbO_2 comes from its anisotropic crystal structure. **Figure 1** schematically represents the unit cell of NbO_2 crystal at room temperature. The crystal structure of NbO_2 is tetragonal and belongs to the space group of $I4_1/a$ with the lattice parameters of a = 1.37 nm and c = 0.599 nm [12]. In NbO_2, the NbO_6 octahedrons are connected at their edges (side lines) along [001] direction whereas they are connected at their corners (end points) in the other directions. Very recently, Kim *et al.* [17] reported that epitaxial NbO_2 films grown on α-Al_2O_3 substrates exhibit anisotropic electron transport: the carrier effective mass (m^*) in $[11\bar{2}]$ direction is 0.05 m_0

whereas that in [$1\bar{1}0$] and [001] directions are much heavier ([$1\bar{1}0$]: ~1 m_0, [001]: ~0.8 m_0). The electron transportation in semiconducting oxides is strongly affected by the electron-phonon collisions, which is related to the vibrational properties of the lattice. In addition, the elasticity tensor of NbO_2 shows anisotropy along its major axes and nonzero off-diagonal terms [18-19]. All physical properties of NbO_2 suggest that its thermal conductivity would be anisotropic.

In this study, we measured the thermal conductivities along [110]-, [001]-, and [111]-directions using the (110)-, (001)-, and (111)-oriented NbO_2 films and found [111]-direction shows ~1 W m^{-1} K^{-1} higher thermal conductivity compared with the other directions. In order to clarify the heat conduction in NbO_2 crystal, we extracted the full thermal conductivity tensor ($\hat{\kappa}$) from the observed thermal conductivities. $\hat{\kappa}$ has 6 independent terms. In case of NbO_2, this can be reduced to 3 independent terms because of its 4-fold symmetry in the *ab*-plane. In a matrix representation, it looks as follows:

$$\hat{\kappa}_{NbO_2} = \begin{pmatrix} \kappa_{11} & \kappa_{12} & \kappa_{13} \\ \kappa_{12} & \kappa_{22} & \kappa_{23} \\ \kappa_{13} & \kappa_{23} & \kappa_{33} \end{pmatrix} \rightarrow \begin{pmatrix} \kappa_{11} & 0 & \kappa_{13} \\ 0 & \kappa_{11} & \kappa_{13} \\ \kappa_{13} & \kappa_{13} & \kappa_{33} \end{pmatrix} \quad \ldots\ldots \quad (1)$$

where the subscripts 1, 2, and 3 refer to *a*-, *b*-, and *c*-axis of NbO_2, respectively. Using the thermal conductivities in three different directions of [110], [001], and [111], we successfully determined $\hat{\kappa}_{NbO_2}$. The components of $\hat{\kappa}_{NbO_2}$ were converted to the total thermal conductivity (κ_{tot}) using tensor coordinate transformations **(Supplementary)**, and the resulting system of non-linear equations were solved to obtain all components of $\hat{\kappa}_{NbO_2}$ (Eq. 1). We believe the present results are significantly important for understanding the heat accumulations in NbO_2 based devices, which are critical for enhancing their performance.

Materials and methods

Using RF magnetron sputtering, NbO_2 films with three different crystallographic orientations were grown on (0001) α-Al_2O_3, (10$\bar{1}$0) α-Al_2O_3 and (1$\bar{1}$02) α-Al_2O_3 substrates (Crystal Bank at Pusan National University), respectively. The films were grown at 650 ºC under 2.5−5 mTorr of Ar/H partial pressure. The details of our NbO_2 film growth condition are described elsewhere [17]. The film thicknesses (*t*) and crystallographic orientations were analyzed by X-ray diffraction (HRXRD, Cu Kα_1 radiation, ATX-G, Rigaku Co.). The total thermal conductivity (κ_{tot}) of the resultant NbO_2 films were measured in the out-of-plane direction with time-domain thermo-reflectance (TDTR, pump beam wavelength: 775 nm, probe beam wavelength: 1550 nm, pulse duration: 1 ps, pulse frequency: 20 MHz method, PicoTR, PicoTherm Co.) at room temperature. Metallic Mo films (~100 nm), which were used as the transducer, were deposited on the top surface of the NbO_2 films by d.c. magnetron sputtering method at room temperature.

Results and discussion

Figure 2 shows the out-of-plane XRD patterns **[Fig. 2(a)]** and the rocking curves (OXRCs) **[Fig. 2(b)]** of the resultant NbO_2 films. Only intense diffraction peaks of 110 (top), 001 (middle), and 111 (bottom) NbO_2 are seen together with the α-Al_2O_3 diffraction peaks in **Fig. 2(a)**, indicating that highly oriented single phase NbO_2 films were grown on the α-Al_2O_3 substrates. Full-width at half maximum (FWHM) of the OXRCs of 440 NbO_2 (top) and 222 NbO_2 (bottom) are ~0.02 °, which corresponds to the resolution of our X-ray diffractometer, indicating strong 110 and 111 orientation of the films while that of 004 NbO_2 (middle) is a bit broader (0.76 °). From these results, the out-of-plane orientation of the

resultant films were clarified as [(110) NbO_2 ‖ (0001) α-Al_2O_3], [(001) NbO_2 ‖ (10$\bar{1}$0) α-Al_2O_3] and [(111) NbO_2 ‖ (1$\bar{1}$02) α-Al_2O_3]. From the X-ray reflection measurements (data not shown), the film thickness of the (110)-, (001)-, and (111)-oriented films were clarified 68, 52, and 72 nm, respectively, which were sufficiently thick for the films to behave like bulk materials (≥ 30 nm, **Supplementary Table S1**) [20].

Figure 3 summarizes the thermo-reflectance signals from the NbO_2 films grown on α-Al_2O_3 substrates at room temperature. Sharp increase and decay curves before ~2 ns are due to the Mo transducer. The decay of (111)-oriented NbO_2 film is slightly faster than (110)- and (001)-oriented NbO_2 films, clearly indicating that κ_{tot} in the (111) direction is higher than that in the (110) and (001) directions. We analyzed the thermo-reflectance decay curves with the software package provided by the manufacturer and obtained the κ_{tot} of 3.0 W m^{-1} K^{-1} for (110), 2.9 W m^{-1} K^{-1} for (001), and 4.0 W m^{-1} K^{-1} for (111), respectively.

Acoustic longitudinal phonons usually dominate the lattice thermal conductivity [21-23]. While the presence of soft phonons in the phonon dispersion relations makes it challenging to obtain detailed phonon transport characteristics of NbO_2 [24], the speed of acoustic longitudinal phonons can be estimated with the its elastic stiffness constants [18-19]. According to our calculations, the speed of elastic longitudinal waves along [111], [110], and [001] are 8476 m s^{-1}, 7978 m s^{-1}, and 8109 m s^{-1}, respectively **(Supplementary)**. Therefore, the high thermal conductivity observed from the (111) oriented film is attributed to the speed of acoustic longitudinal phonons. We would like to note that the

observed thermal conductivities are not proportional to the calculated acoustic longitudinal phonon speeds, and the calculation results only explain why (111) film shows the highest thermal conductivity. To fully explain the observed thermal conductivities, it is necessary to understand the coupling of soft phonons, which are mainly populated near *P* point (Brillouin Zone edge along [111]). Since these phonons are shear waves along [111] with large displacement fields [7], one possibility is anisotropic soft phonon scattering effect. In this scenario, soft phonon scattering would reduce the thermal transport properties along [001] and [110] films whereas its effect on the [111] longitudinal waves will be relatively small since their displacement fields ([111] longitudinal and transverse) are perpendicular. At elevated temperatures, as phonon softening will be compensated by an increase in the phonon population, the soft phonon effect will be enhanced, and the anisotropy will likely increase.

The observed thermal conductivity κ_{tot} is sum of the lattice thermal conductivity (κ_{lat}) and the electron thermal conductivity (κ_{ele}). In order to estimate the maximum contribution of carrier electrons (κ_{ele}) to the observed κ_{tot}, we measured the in-plane electrical resistivity (ρ) of the NbO_2 films by the d.c. four-probe method in van der Pauw electrode configuration at room temperature (**Table I**). The ρ values of (110)-, (001)-, and (111)-oriented films were 51, 2, and 51 Ω cm, respectively. Using these ρ values, we estimated κ_{ele} assuming the Wiedemann-Franz law ($\kappa_{ele} = L \cdot \sigma \cdot T$, where L is the Lorenz number of a free electron gas (2.45×10^{-8} W Ω^{-1} K^{-2}) [25], σ is the electrical conductivity ($=\rho^{-1}$), and T is the absolute temperature). While the Wiedemann-Franz law is often not suitable for describing mobile electrons in oxides [26], it does offer reasonable estimations for the upper bound for κ_{ele}. Note that the κ_{ele} values are negligibly small ($< 4 \times 10^{-4}$ W m^{-1} K^{-1}) as compared with κ_{tot}. Therefore, we concluded that the heat transportation in NbO_2 crystal is mostly dominated by lattice vibrations (≡phonons, κ_{lat}).

The ρ of (110) and (111) oriented NbO_2 films are within agreements with our previous studies [17]. However, the ρ of (001) film was noticeably lower than that of the other two films. This implies the presence of oxygen vacancies [27], which may be attributed to the large lattice mismatch (1.75 % and 10.6 %) between the $(10\bar{1}0)$ α-Al_2O_3 substrate and (001) NbO_2 [12, 28]. As oxygen vacancies can affect the thermal conductivity [29-30], their effects must be quantified to avoid mischaracterizing $\hat{\kappa}_{NbO_2}$. To examine the effect of oxygen vacancies on κ_{tot} of our NbO_2 films, we slightly adjusted the sputter deposition condition to fabricate oxygen deficient NbO_{2-x} films and measured their thermal conductivities **(Supplementary Table S1)**. The ρ values of NbO_{2-x} films were orders of magnitude lower than the ρ values in **Table I**, but κ_{tot} values remained almost unchanged. These results confirm that the effect oxygen deficiency on the κ_{tot} of our NbO_2 films is negligibly small.

Here we show the thermal conductivity tensor, $\hat{\kappa}_{NbO_2}$. Equation (1) describes $\hat{\kappa}_{NbO_2}$ when the *c*-axis of the film is perpendicular to its top surface. Since the orientations of the NbO_2 films are not identical, $\hat{\kappa}_{NbO_2}$ needs to be transformed accordingly to properly interpret κ_{tot} observed from differently oriented films. The following matrices represent $\hat{\kappa}_{NbO_2}$ of (110) and (111) oriented films in a Cartesian coordinate when $\hat{z}$-axis is perpendicular to the substrate **(See Supplementary information)**:

$$\hat{\kappa}_{NbO_2,(110)} = \begin{pmatrix} \kappa_{33} & 0 & \sqrt{2}\kappa_{13} \\ 0 & \kappa_{11} & 0 \\ \sqrt{2}\kappa_{13} & 0 & \kappa_{11} \end{pmatrix} \quad \ldots\ldots \quad (2a)$$

$$\hat{\kappa}_{NbO_2,(111)} = \begin{pmatrix} \frac{1}{3}(\kappa_{11} - 4\kappa_{13} + 2\kappa_{33}) & 0 & \frac{\sqrt{2}}{3}(\kappa_{11} - \kappa_{13} - \kappa_{33}) \\ 0 & \kappa_{11} & 0 \\ \frac{\sqrt{2}}{3}(\kappa_{11} - \kappa_{13} - \kappa_{33}) & 0 & \frac{1}{3}(2\kappa_{11} + 4\kappa_{13} + \kappa_{33}) \end{pmatrix} \quad \ldots\ldots \quad (2b)$$

where $\hat{\kappa}_{NbO_2,(hkl)}$ represents the thermal conductivity tensor of the (*hkl*)-oriented NbO_2 film. The heat flux $\vec{j}$ in the film induced by the temperature gradient $\vec{\nabla}T$ across the film can be written as:

$$\vec{j} = -\hat{\kappa}_{NbO_2,(hkl)}\vec{\nabla}T \qquad \ldots\ldots \qquad (3)$$

During TDTR measurements, the pump laser creates a temperature difference across the film, and the resulting signal reflects the total heat flux leaving the top surface. Therefore, $\vec{\nabla}T$ = (0, 0, ∇T) and $\kappa_{tot} = |\vec{j}|/\nabla T$. This yields 3 different coupled non-linear equations **(See Supplementary information)**:

$$\kappa_{tot[001]} = \sqrt{{k_{33}}^2 + 2{k_{13}}^2} = 2.9 \text{ W m}^{-1} \text{ K}^{-1} \qquad \ldots\ldots \qquad (4a)$$

$$\kappa_{tot[110]} = \sqrt{{k_{11}}^2 + 2{k_{13}}^2} = 3.0 \text{ W m}^{-1} \text{ K}^{-1} \qquad \ldots\ldots \qquad (4b)$$

$$\kappa_{tot[111]} = \frac{1}{3}\sqrt{2(k_{11} - k_{13} - k_{33})^2 + (2k_{11} + 4k_{13} + k_{33})^2} = 4.0 \text{ W m}^{-1} \text{ K}^{-1} \qquad \ldots\ldots \qquad (4c)$$

Equations (4a−4c) have two different sets of solutions: (k_{11}, k_{13}, k_{33})= (2.60, 1.06, 2.48) W m^{-1} K^{-1} and (1.60, 1.79, 1.41) W m^{-1} K^{-1}. In this case, elasticity can be used to choose a more appropriate solution since propagation of elastic waves can be reasonable estimations for the propagation of phonons. According to previous studies, the terms in the elasticity of NbO_2 representing compression/tension are always greater than the terms representing shear [19]. This suggests the latter solution needs to be discarded since its off-diagonal term is greater than the two diagonal terms, which is highly unlikely. Therefore, if *a*-, b-, and *c*-axes of the NbO_2 unit cell are used as the Cartesian axes, $\hat{\kappa}_{NbO_2}$ is expressed by the following matrix:

$$\hat{\kappa}_{NbO_2} = \begin{pmatrix} 2.60 & 0 & 1.06 \\ 0 & 2.60 & 1.06 \\ 1.06 & 1.06 & 2.48 \end{pmatrix} \text{ W m}^{-1} \text{ K}^{-1} \text{ (@ 300K)} \qquad \ldots\ldots \qquad (4)$$

Using the $\hat{\kappa}_{NbO_2}$, one can calculate the heat flux in NbO_2 along any directions, which is useful for understanding the heat flux in NbO_2 based devices.

Conclusion

In summary, we successfully clarified the full thermal conductivity tensor of NbO_2 for the first time using the thermal conductivity values of (001)-, (110)-, and (111)-oriented NbO_2 films grown on α-Al_2O_3 substrates. Using the (110)-, (001)-, and (111)-oriented NbO_2 films, we measured the thermal conductivity of [110]-, [001]-, and [111]-directions and found [111]-direction shows ~1 W m^{-1} K^{-1} higher thermal conductivity compared with the other directions (~3 W m^{-1} K^{-1}). The diagonal components of the thermal conductivity tensor were ~2.5 W m^{-1} K^{-1} while the nonzero off-diagonal component was ~1 W m^{-1} K^{-1}. These results will be essential for understanding the flow of heat in NbO_2 based devices, which is critical for their design and efficiency optimization.

Acknowledgements

H.J. and H.O. are supported by the Korea-Japan bilateral program funded from following programs of each country: International cooperation program by the NRF (NRF-2018K2A9A2A08000079) and JSPS. H.O. is supported by Grants-in-Aid for Scientific Research A (17H01314) from the JSPS, the Asahi Glass Foundation, and the Mitsubishi Foundation.

Table I | Anisotropic thermal conductivity of the NbO_2 films at room temperature. Total thermal conductivity (κ_{tot}) in the out-of-plane direction, in-plane resistivity (ρ), and electron thermal conductivity (κ_{ele}) assumed with Wiedemann-Franz law of the (110)-, (001)-, and (111)-oriented NbO_2 films are listed. (111)-oriented film shows higher κ_{tot} compared with (110)- and (001)-oriented films. Note that the κ_{ele} values are negligibly small compared to κ_{tot}.

Orientations	t (nm)	κ_{tot} (out-of-plane, $W \cdot m^{-1} \cdot K^{-1}$)	ρ (in-plane, $\Omega \cdot cm$)	κ_{ele} ($W \cdot m^{-1} \cdot K^{-1}$)
(110)	68	3.0	51	1.4×10^{-5}
(001)	52	2.9	2	3.7×10^{-4}
(111)	72	4.0	51	1.4×10^{-5}

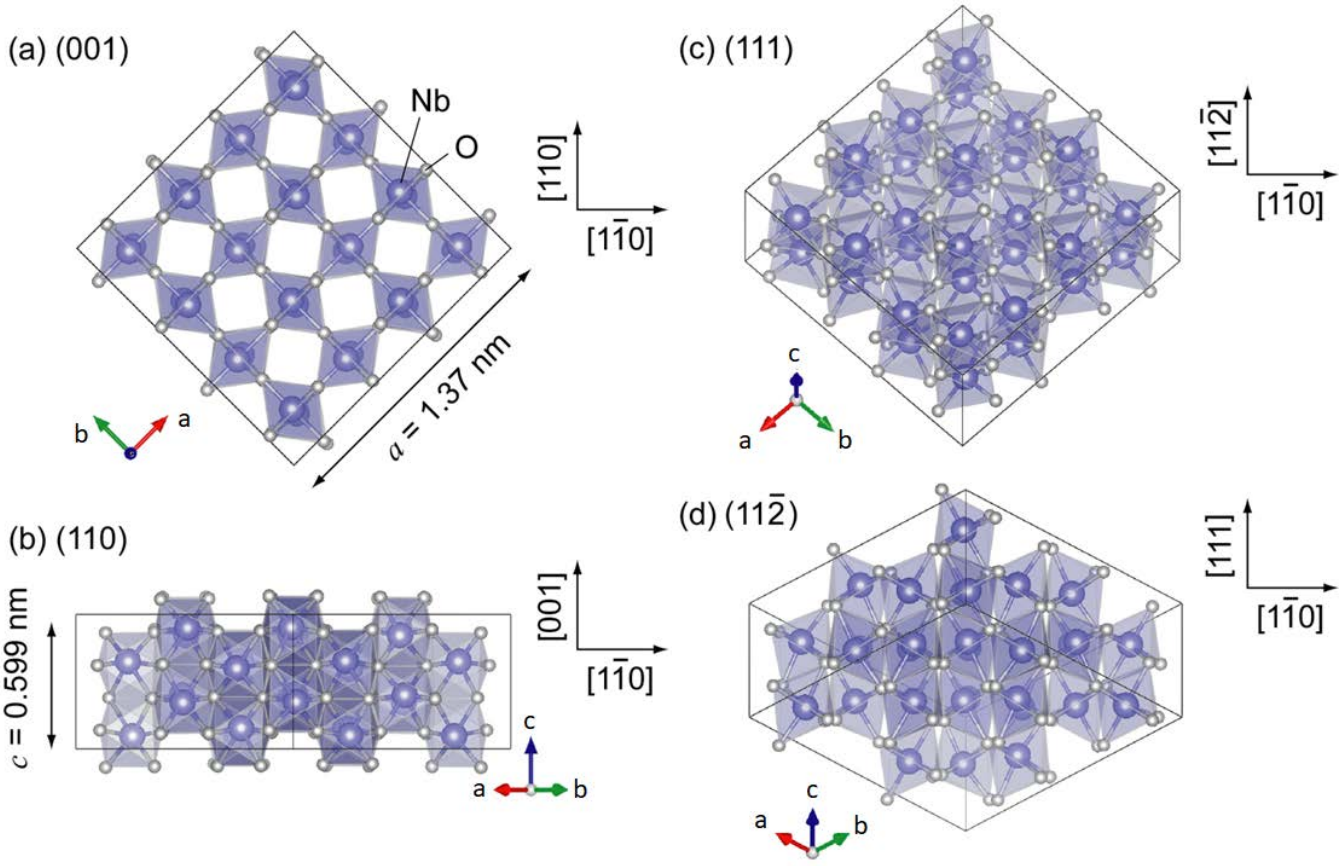

Figure 1 | Schematic crystal structure of NbO_2 at room temperature. Projection along the normal to (a) (001), (b) (110), (c) (111), and (d) [11-2]. The space group is $I4_1/a$ and the lattice parameters are a = 1.37 nm and c = 0.599 nm [12]. Note that the NbO_6 octahedrons are connected at their edges (side lines) in [001] direction whereas they are connected at their corners (end points) in other directions.

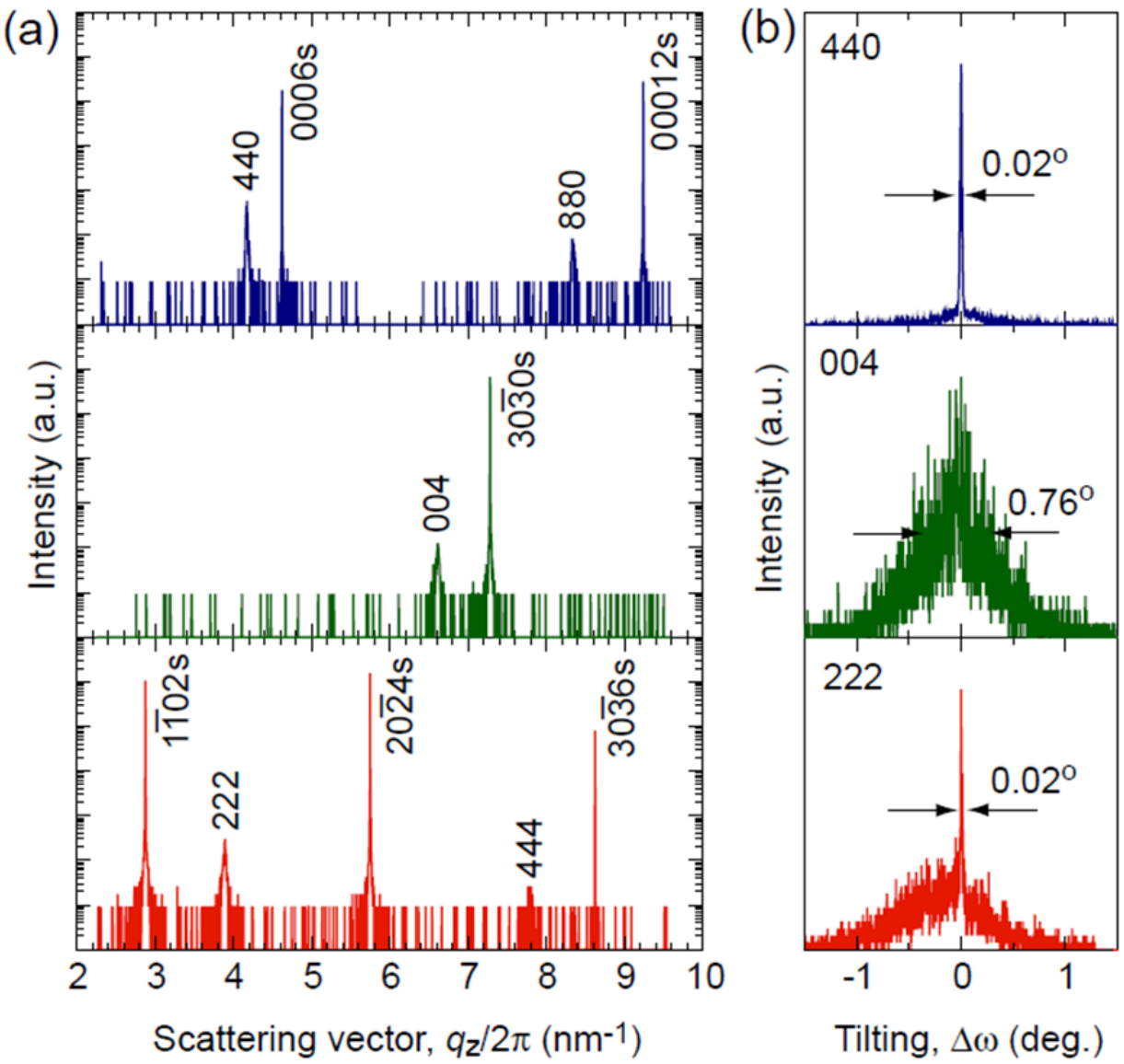

FIG. 2 | Crystallographic orientation of the resultant NbO_2 films. (a) Out-of-plane X-ray Bragg diffraction patterns and (b) corresponding out-of-plane X-ray rocking curves (OXRCs) of the resultant NbO_2 films. Only intense diffraction peaks of 110 (top), 001 (middle), and 111 (bottom) NbO_2 are seen together with the α-Al_2O_3 diffraction peaks in (a), indicating that highly oriented single phase NbO_2 films were grown on the α-Al_2O_3 substrates. FWHM of the OXRCs of 440 NbO_2 (top) and 222 NbO_2 (bottom) are ~0.02 °, which corresponds to the resolution of our X-ray diffractometer, indicating strong 110 and 111 orientation of the films, while that of 004 NbO_2 (middle) is a bit broader (0.76 °).

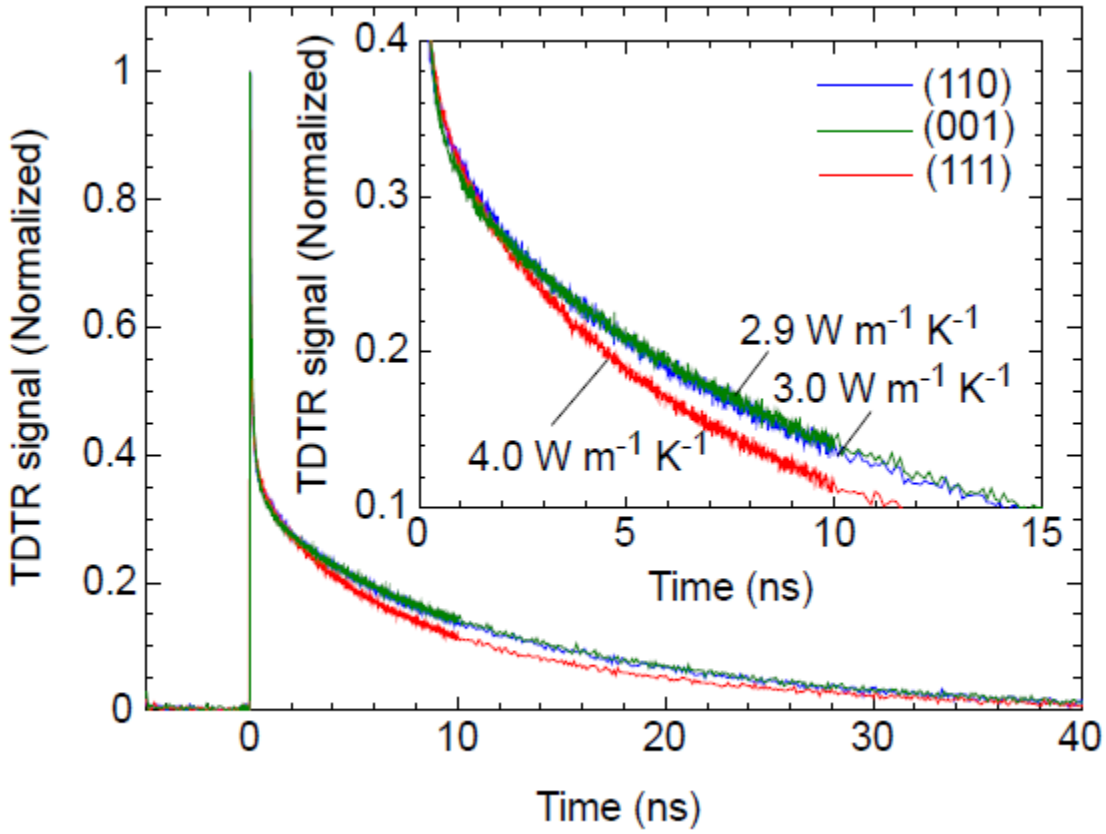

FIG. 3 | Thermo-reflectance signal of the NbO_2 films grown on α-Al_2O_3 substrates at room temperature. Sharp increase and decay curves until ~2 ns are due to the Mo transducer. The decay of (111)-oriented NbO_2 film is slightly faster than (110)- and (001)-oriented NbO_2 films, clearly indicating that κ_{tot} in the (111) direction is higher than that in the (110) and (001) directions. Using these thermo-reflectance decay curves, we obtained the κ_{tot} of 3.0 W m^{-1} K^{-1} for (110), 2.9 W m^{-1} K^{-1} for (001), and 4.0 W m^{-1} K^{-1} for (001), respectively.

References

1. Park, J.; Hadamek, T.; Posadas, A. B.; Cha, E.; Demkov, A. A.; Hwang, H., Multi-layered $NiO_y/NbO_x/NiO_y$ fast drift-free threshold switch with high I_{on}/I_{off} ratio for selector application. *Scientific Reports* **2017,** *7* (1), 4068.
2. Nandi, S. K.; Liu, X.; Venkatachalam, D. K.; Elliman, R. G., Threshold current reduction for the metal–insulator transition in NbO_{2-x}-selector devices: the effect of ReRAM integration. *Journal of Physics D: Applied Physics* **2015,** *48* (19), 195105.
3. Lee, M. J.; Park, Y.; Suh, D. S.; Lee, E. H.; Seo, S.; Kim, D. C.; Jung, R.; Kang, B. S.; Ahn, S. E.; Lee, C. B., Two series oxide resistors applicable to high speed and high density nonvolatile memory. *Advanced Materials* **2007,** *19* (22), 3919-3923.
4. Son, M.; Lee, J.; Park, J.; Shin, J.; Choi, G.; Jung, S.; Lee, W.; Kim, S.; Park, S.; Hwang, H., Excellent selector characteristics of nanoscale VO_2 for high-density bipolar ReRAM applications. *IEEE Electron Device Letters* **2011,** *32* (11), 1579-1581.
5. Wong, H.-S. P.; Lee, H.-Y.; Yu, S.; Chen, Y.-S.; Wu, Y.; Chen, P.-S.; Lee, B.; Chen, F. T.; Tsai, M.-J., Metal–oxide RRAM. *Proceedings of the IEEE* **2012,** *100* (6), 1951-1970.
6. Pickett, M. D.; Medeiros-Ribeiro, G.; Williams, R. S., A scalable neuristor built with Mott memristors. *Nature materials* **2013,** *12* (2), 114.
7. Joshi, T.; Senty, T. R.; Borisov, P.; Bristow, A. D.; Lederman, D., Preparation, characterization, and electrical properties of epitaxial NbO_2 thin film lateral devices. *Journal of Physics D: Applied Physics* **2015,** *48* (33), 335308.
8. Kang, M.; Yu, S.; Son, J., Voltage-induced insulator-to-metal transition of hydrogen-treated NbO_2 thin films. *Journal of Physics D: Applied Physics* **2015,** *48* (9), 095301.
9. Kang, M.; Son, J., Off-state current reduction in NbO_2-based selector device by using TiO_2 tunneling barrier as an oxygen scavenger. *Applied Physics Letters* **2016,** *109* (20), 202101.
10. Kumar, S.; Strachan, J. P.; Williams, R. S., Chaotic dynamics in nanoscale NbO_2 Mott memristors for analogue computing. *Nature* **2017,** *548* (7667), 318-321.
11. Sakata, T.; Sakata, K.; Nishida, I., Study of phase transition in NbO_2. *Physica Status Solidi B: Basic Research* **1967,** *20* (2), 155-157.
12. Bolzan, A. A.; Fong, C.; Kennedy, B. J.; Howard, C. J., A powder neutron diffraction study of semiconducting and metallic niobium dioxide. *Journal of Solid State Chemistry* **1994,** *113* (1), 9-14.
13. Chopra, K., Current-controlled negative resistance in thin niobium oxide films. *proceedings of the IEEE* **1963,** *51* (6), 941-942.
14. Chudnovskii, F.; Odynets, L.; Pergament, A.; Stefanovich, G., Electroforming and switching in oxides of transition metals: The role of metal–insulator transition in the switching mechanism. *journal of Solid State Chemistry* **1996,** *122* (1), 95-99.
15. Bae, J.; Hwang, I.; Jeong, Y.; Kang, S.-O.; Hong, S.; Son, J.; Choi, J.; Kim, J.; Park, J.; Seong, M.-J., Coexistence of bi-stable memory and mono-stable threshold resistance switching phenomena in amorphous NbOx films. *Applied Physics Letters* **2012,** *100* (6), 062902.
16. Jung, K.; Kim, Y.; Jung, W.; Im, H.; Park, B.; Hong, J.; Lee, J.; Park, J.; Lee, J.-K., Electrically induced conducting nanochannels in an amorphous resistive switching niobium oxide film. *Applied Physics Letters* **2010,** *97* (23), 233509.
17. Kim, G.; Zhang, Y. Q.; Min, T.; Suh, H.; Jang, J. H.; Kong, H.; Lee, J.; Lee, J.; Jeon, T. Y.; Lee, I.; Cho, J.; Ohta, H.; Jeen, H., Extremely Light Carrier‐Effective Mass in a Distorted Simple Metal Oxide. *Advanced Electronic Materials* **2019,** *5*, 1800504.
18. Boyle, W.; Bennett, J.; Shin, S.; Sladek, R., Elastic constants of NbO_2 at room temperature. *physical review B* **1976,** *14* (2), 526.

19. Rimai, D.; Sladek, R., Comment on the elastic properties of semiconducting NbO_2. *Physical Review B* **1978,** *18* (6), 2944.
20. Costescu, R. M.; Wall, M. A.; Cahill, D. G., Thermal conductance of epitaxial interfaces. *physical review B* **2003,** *67* (5), 054302.
21. Ju, Y. S.; Goodson, K. E., Phonon scattering in silicon films with thickness of order 100 nm. *Applied Physics Letters* **1999,** *74*, 3005-3007.
22. Narumanchi, S. V.; Murthy, J.; Amon, C. H., Comparison of different phonon transport models for predicting heat conduction in silicon-on-insulator transistors. *Journal of Heat Transfer* **2005,** *127* (7), 713-723.
23. Sood, K. C.; Roy, M. K., Longitudinal phonons and high-temperature heat conduction in germanium. *Journal of Physics: Condensed Matter* **1993,** *5*, 301-312.
24. O'Hara, A.; Demkov, A. A., Nature of the metal-insulator transition in NbO_2. *Physical Review B* **2015,** *91*, 094305.
25. Kittel, C., *Introduction to solid state physics*. Wiley New York: 1976; Vol. 8.
26. Lee, S.; Hippalgaonkar, K.; Yang, F.; Hong, J.; Ko, C.; Suh, J.; Liu, K.; Wang, K.; Urban, J. J.; Zhang, X., Anomalously low electronic thermal conductivity in metallic vanadium dioxide. *Science* **2017,** *355* (6323), 371-374.
27. Onozato, T.; Katase, T.; Yamamoto, A.; Katayama, S.; Matsushima, K.; Itagaki, N.; Yoshida, H.; Ohta, H., Optoelectronic properties of valence-state-controlled amorphous niobium oxide. *Journal of Physics: Condensed Matter* **2016,** *28* (25), 255001.
28. Wong, F. J.; Ramanathan, S., Heteroepitaxy of distorted rutile-structure WO_2 and NbO_2 thin films. *Journal of Materials Research* **2013,** *28* (18), 2555-2563.
29. Luckyanova, M. N.; Chen, D.; Ma, W.; Tuller, H. L.; Chen, G.; Yildiz, B., Thermal conductivity control by oxygen defect concentration modification in reducible oxides: The case of $Pr_{0.1}Ce_{0.9}O_{2-\delta}$ thin films. *Applied physics letters* **2014,** *104* (6), 061911.
30. Wu, X.; Walter, J.; Feng, T.; Zhu, J.; Zheng, H.; Mitchell, J. F.; Biškup, N.; Varela, M.; Ruan, X.; Leighton, C., Glass‐Like Through‐Plane Thermal Conductivity Induced by Oxygen Vacancies in Nanoscale Epitaxial $La_{0.5}Sr_{0.5}CoO_{3-\delta}$. *Advanced Functional Materials* **2017,** *27* (47), 1704233.